Biosensors and Bioelectronics 134 (2019) 42–48

Contents lists available at ScienceDirect

Biosensors and Bioelectronics

journal homepage: www.elsevier.com/locate/bios

Simple "signal-on" photoelectrochemical aptasensor for ultrasensitive detecting AFB1 based on electrochemically reduced graphene oxide/poly(5-formylindole)/Au nanocomposites

Bin Zhang, Yan Lu, Chaonan Yang, Qingfu Guo, Guangming Nie*

Key Laboratory of Optic-Electric Sensing and Analytical Chemistry for Life Science, MOE, Key Laboratory of Analytical Chemistry for Life Science in Universities of Shandong, Shandong Key Laboratory of Biochemical Analysis, College of Chemistry and Molecular Engineering, Qingdao University of Science and Technology, Qingdao, 266042, PR China

ARTICLE INFO

Keywords:
Photoelectrochemistry
Aptasensor
Nanocomposites
Polyindole
Aflatoxin B1

ABSTRACT

A simple "signal-on" photoelectrochemical (PEC) aptasensor is constructed for Aflatoxin B1 (AFB1) detection based on electrochemically reduced graphene oxide/poly(5-formylindole)/Au (erGO/P5FIn/Au) nanocomposites. The nanocomposites are synthesized by simple electrochemical deposition method and show good photoelectrochemical performance. Poly(5-formylindole) (P5FIn) can generate electron-hole pairs under light irradiation, leading to the formation of robust cathode photocurrent. Au can be acted as signal amplifier due to the high conductivity. The erGO is used to immobilize AFB1 aptamer chain by π-π stacking interaction between the carbon six-membered ring in graphene and the C-N heterocyclic ring in nucleobases of ssDNA. After the insulating AFB1 aptamer chain is fixed to the electrode, the signal of PEC sensor is "OFF". In the process of AFB1 detection, the aptamer chain detaches from the surface of erGO, which results in "ON" of the sensor signal. Based on this design, this constructed PEC aptasensor shows a high sensitivity for AFB1 with a wide linear detection range (LDR) from 0.01 ng mL^{-1} to 100 ng mL^{-1}. The limit of detection (LOD) is 0.002 ng mL^{-1}. This PEC sensor also exhibits good stability, selectivity, specificity, and satisfactory practical sample analysis ability. This work may provide a new promising PEC platform for AFB1 detection as well as some other small molecules analysis.

1. Introduction

Food safety issues have aroused more and more attention with the development of society (Vasilescu and Marty, 2016). Aflatoxin B1 (AFB1), one of the necessary food testing items, has strong carcinogenic effect (Xu et al., 2014). Many countries have established relevant laws to regulate the content of AFB1 in food. For example, permissible levels set by China and the United States are 20 ng mL^{-1}. In European Union, the maximum allowed level is 5 ng mL^{-1} for rice and 2 ng mL^{-1} for dried fruits. In Korea and Japan, the maximum allowed level is 1 ng mL^{-1} (Liu et al., 2013; Zhang et al., 2011). Many analytical methods have been reported for detecting AFB1, such as high performance liquid chromatography (HPLC) (Tang et al., 2014), liquid chromatography-mass spectrometry (LC-MS) (Wang et al., 2013; Kong et al., 2014), and electrochemiluminescence (ECL) immunosensors (Wang et al., 2018). These methods have high selectivity, but they require complicated procedures, heavy equipment, and complex operation. The disadvantages of these analytical methods limit its practical application in some degree. Therefore, it is necessary to design and prepare some simple, low power consumption, low cost and sensitive sensor for AFB1 detection (Gu and Zhang, 2018).

Photoelectrochemical (PEC) sensing technology as a new detection method has attracted more and more attentions of researchers (Zang et al., 2017). In the PEC detection process, light acts as excitation source. And the photocurrent generated on the electrode is used as detection signal (Hou et al., 2017, Pardo-Yissar et al., 2003). PEC sensors have electrochemical and optical advantages due to the combination of photoirradiation and electrochemical detection (Ma et al., 2013). On one hand, the complete separation of the excitation source and detecting signal ensures that PEC sensors have a low background signal and a high sensitivity (Li et al., 2016). On the other hand, the application of electrochemical technology makes PEC instruments simple, compact, low power consumption and low cost (Ge et al., 2013). Therefore, PEC sensing analysis technology plays an increasingly important role in chemical and biological analysis. There are two main detection types in PEC analysis, "signal-off" and "signal-on" (Hao et al.,

* Corresponding author.
E-mail addresses: gmnie@126.com, gnie@qust.edu.cn (G. Nie).

https://doi.org/10.1016/j.bios.2019.03.048
Received 16 January 2019; Received in revised form 19 March 2019; Accepted 23 March 2019
Available online 28 March 2019

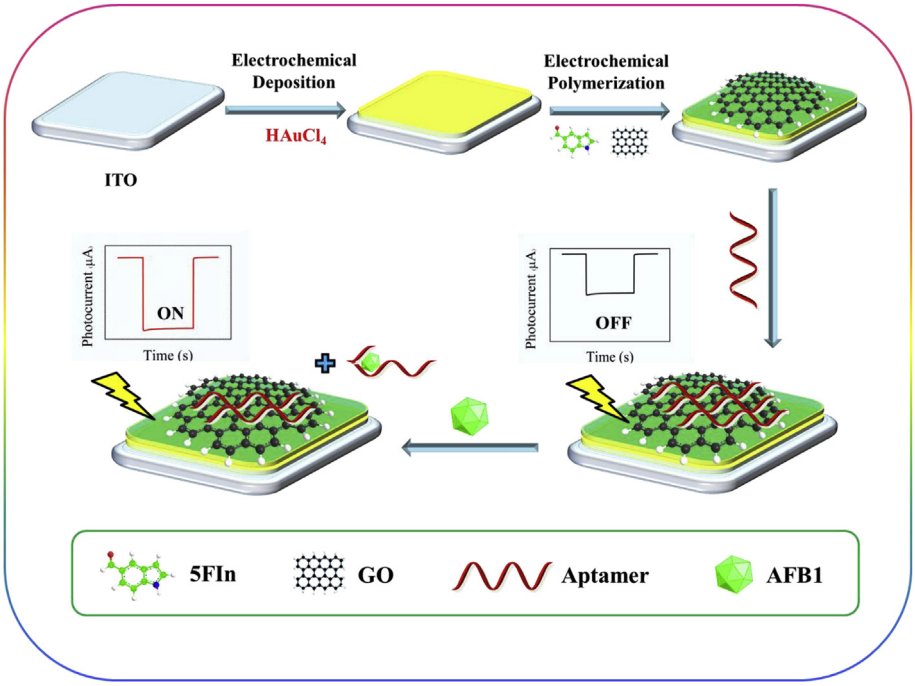

Scheme 1. Schematic illustration of PEC aptasensor.

2017). In the previous works, the prepared PEC sensors were commonly "signal-off" type to reach the detecting aim, where the insulative property of markers can usually hinder electron transfer and reduce the response of PEC sensor (Liu et al., 2018). Compared with the "signal-off" type PEC sensor, "signal-on" type can reduce the false response generated during detection process and obtain a more precise result owing to its low background signal (Chen and Zhao, 2017). Now, the photoactive materials used in PEC sensor are mainly derived from metal semiconductor materials (such as CdS, TiO_2, CdSe, and CdTe), which have high-efficiency photoelectric conversion properties (Zhuang et al., 2015a,b). However, the practical application of metal semiconductors in PEC analysis is still limited for two reasons. Firstly, semiconductor materials, such as CdSe and CdTe have high toxicity and poor stability (Lin et al., 2016). Secondly, some semiconductors with wide band gaps (SnO_2 is 3.5 eV and ZnO is 3.2 eV) have strong oxidation properties and require high energy excitation sources (Zhuang et al., 2015a,b; Fan et al., 2014). Thus, finding novel photosensitive materials with high-efficiency, non-toxic, low-energy excitation and low-cost is a crucial challenge for further improvement of the efficiency and application of PEC system.

In recent years, nanocomposites based on conducting polymers (CPs) have been extensively studied because of its excellent properties in the field of electricity and optics (Nie et al., 2007, 2011). Some CPs were applied to PEC sensors, such as polyaniline, polythiophene and polypyrrole (Zhu et al., 2015; Li et al., 2014a,b; Liu et al., 2016). In the polyindole family, poly(5-formylindole) (P5FIn) is a promising candidate of photoactive material because it has high photoelectric activity, good stability and biocompatibility. The photoelectric properties of polyindole can be improved by aldehyde group, which is advantageous for application in PEC analysis (Nie et al., 2018). Compared with traditional inorganic semiconductor materials, P5FIn has some advantages, such as good stability, strong biocompatibility and high conductivity. In addition, P5FIn has a narrower band gap, which is beneficial to its excitation under visible light. Au is widely used in the fields of optics, electricity and biomedicine because of its unique physical and chemical properties. Electrochemically reduced graphene oxide (erGO) is often used as electron acceptor in the PEC field because it can accelerate electron transfer and inhibit electron-hole recombination. Compared with single components, nanocomposite materials have better physical or chemical properties. For example, Au nanocomposites have a very large surface area, good conductivity and excellent porosity, which can be used in the detection of DNA (Spain et al., 2013). Luo et al. designs bio-interfacing PEDOT/GO nanocomposites, which shows good conductivity, minimal cytotoxicity and excellent modifiability (Luo et al., 2013). When the CPs are combined with other materials, its stability, electrochemical performance and optical properties are significantly improved. Therefore, the CPs based nanocomposites have a better application in the field of bioanalysis than single components.

In this work, the electrochemically reduced graphene oxide/poly(5-formylindole)/Au (erGO/P5FIn/Au) nanocomposites with strong photocurrent response are prepared. In order to achieve a simple, sensitive and high specific detection of AFB1, a novel "signal-on" PEC aptasensor based on erGO/P5FIn/Au nanocomposites was developed. In this aptasensor, Au can effectively accelerate electron transfer, improving photo-electric conversion efficiency of P5FIn. erGO can be used to immobilize AFB1 aptamer chain by π–π stacking interaction due to the π-conjugated structure. When AFB1 is specifically bound to the aptamer chain, the AFB1 aptamer chain can be detached from the electrode surface. This leads to the enhancement of the photocurrent results, which means "ON" of the sensor signal. This constructed PEC aptasensor has satisfactory performance in AFB1 detection and actual sample analysis.

2. Experimental

The reagents and apparatus used in this experiment, the details of PEC measurement and actual sample preparation are all described in the Supporting Information.

The preparation process of the PEC aptasensor is exhibited in Scheme 1. Firstly, Au was deposited on the surface of ITO electrode by constant charge method (potential: −1.4 V *vs*. Ag/AgCl, charge: 10 mC) in 1 wt % $HAuCl_4$ solution. Then, P5FIn was deposited on Au/ITO by constant charge method (potential: 1.35 V *vs*. Ag/AgCl, charge: 20 mC) in 5 mL acetonitrile (ACN) solution containing 5-formylindole (0.05 M, 5 FIn) monomer and tetrabutylammonium tetrafluoroborate (0.1 M,

TBATFB). The erGO was introduced into the P5FIn/Au/ITO surface in graphene oxide sol solution by the constant charge method (potential: −1.5 V *vs*. Ag/AgCl, charge: 20 mC). Then 20 μL of 5 μM AFB1 aptamer chain solution was dropwise added onto the erGO/P5FIn/Au/ITO modified electrode surface and stored for 12 h at room temperature. The unbound aptamer chain was removed by deionized water. The AFB1 aptamer chain was modified by π-π stacking (Lu et al., 2015) onto the electrode surface resulting in sensor signal "OFF". Then, the modified electrode was incubated with different concentrations of AFB1 at 25 °C for 70 min. The affinity reaction between AFB1 and the aptamer chain on the surface of the modified electrode resulted in the detachment of AFB1 aptamer chain from the electrode surface. At this moment, the signal of the sensor turned to "ON". The prepared AFB1/Aptamer/erGO/P5FIn/Au/ITO modified electrodes were stored at 4 °C until the use for PEC measurements. The details of preparation and characterizations of erGO/P5FIn/Au nanocomposites are shown in the Supporting Information.

3. Results and discussion

3.1. Characterizations of erGO/P5FIn/Au nanocomposites

The SEM of Au, P5FIn/Au and erGO/P5FIn/Au are shown in Fig. 1, respectively. First of all, Au, P5FIn/Au and erGO/P5FIn/Au materials are prepared on the ITO electrodes by electrochemical deposition, respectively. Then, the prepared Au/ITO, P5FIn/Au/ITO and erGO/P5FIn/Au/ITO electrodes are divided into small pieces. Next, the SEM images are characterized by scanning electron microscope. As shown in Fig. 1A, Au forms a dense film on the surface of the ITO electrode and shows large nanoflower-like structures. Au nanoflower has a large specific surface area, which provides a good platform for P5FIn immobilization. The micro-morphology of P5FIn/Au nanocomposites are shown in Fig. 1B. P5FIn is grown with gold nanoparticles as the core. And the prepared P5FIn/Au nanocomposites shows a nano-fiber structure, which can not only promote the transmission of electrons, but also increase the specific surface of polymer. This nano-fiber structure also provides an excellent platform for the loading of erGO (Groenendaal et al., 2003). From Fig. 1C, it can be seen that erGO is successfully composited with P5FIn/Au on the surface. Because of the high electronic transfer capability and large surface area, erGO can increase the conductivity of the material and load a large number of ssDNA strands. This sandwich-type nanocomposite material exerts the advantages of each component, and further increases the photocurrent intensity of the nanocomposite material owing to the bidirectional acceleration of electron transfer. Therefore, this nanocomposite material may have high photocurrent intensity and photoelectric conversion efficiency, which is favorable for constructing a PEC aptasensor platform.

To further illustrate the successful preparation, the nanocomposites are also characterized by UV-visible absorption spectrum. Au, erGO, P5FIn, P5FIn/Au, erGO/P5FIn/Au nanocomposites are electrodeposited on ITO electrodes, respectively. Then, the samples are rinsed with deionized water before characterizations. UV-visible absorption spectra are illustrated in Fig. 1 D. As shown by curve a (Fig. 1 D), Au exhibits a broad absorption peak at 650 nm. erGO has a strong absorption peak at 360 nm (curve b). The formation of this absorption peak can be attributed to the excitation of the π bond structure of erGO. The main absorption P5FIn is between 380 and 400 nm (curve c) caused by π-π* transition behavior. Two absorption peaks are also observed in curve d, which are different from other peak patterns. This phenomenon indicates that P5FIn/Au is successfully prepared. Moreover, the absorption spectrum of the P5FIn/Au nanocomposites is extended to the

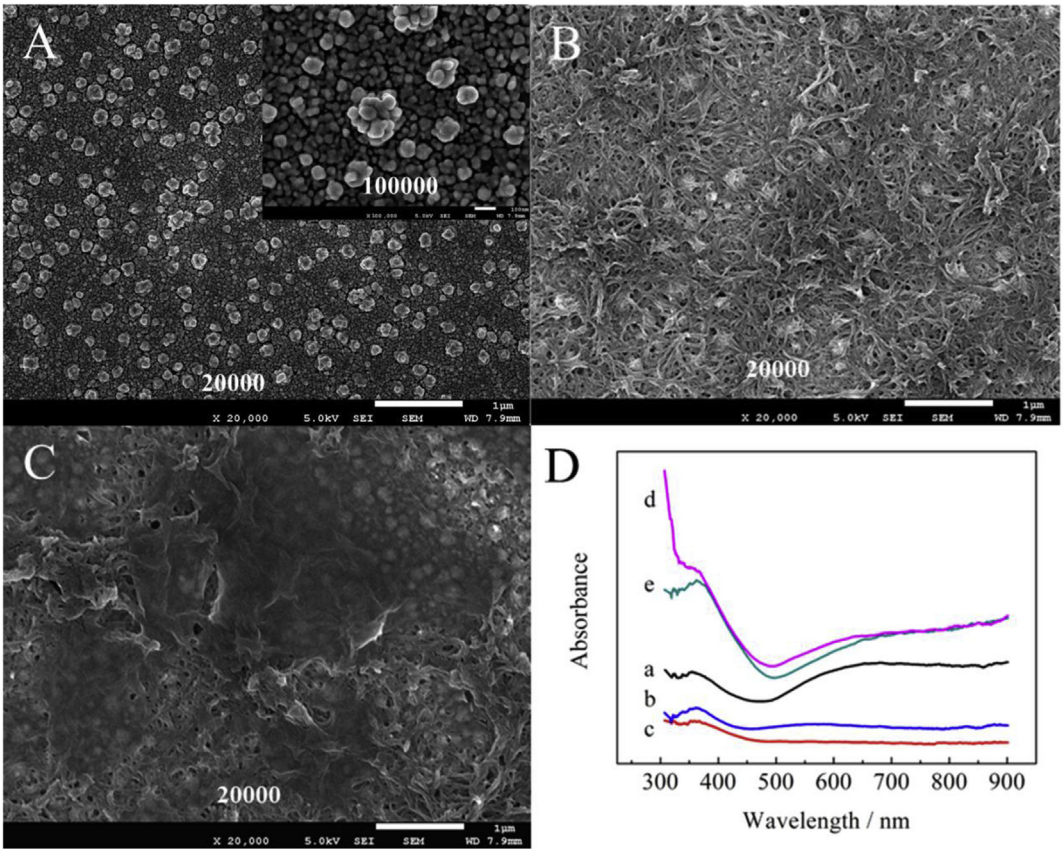

Fig. 1. SEM of (A) Au, (B) P5FIn/Au, (C) erGO/P5FIn/Au nanocomposites and (D) UV-visible absorption spectra of (a) Au, (b) erGO, (c) P5FIn, (d) P5FIn/Au, (e) erGO/P5FIn/Au nanocomposites.

visible region due to the doping of Au particles into the framework of the polymer. The expansion of the absorption range is beneficial to improve the PEC performance of the P5FIn/Au composites. A slight red shift of the two absorption peaks can be observed from the curve e when erGO is introduced into the surface of the P5FIn/Au composites. This phenomenon may be caused by the increased binding sites of nanocomposites. All these data indicates that erGO/P5FIn/Au nanocomposites with large specific surface area have been successfully prepared.

3.2. Characterizations of the PEC aptasensor

The photocurrent response is an important method for studying the charge transfer and separation rate of the photoactive materials. The initial photocurrent response is generated by separation of photogenerated electron-hole pairs of photoactive material. Subsequently, photogenerated electrons are transferred to the transmission contact points. And then the substances in the electrolyte can capture the electrons. When the electron yield is equal to recombination rate, the photocurrent intensity is in a stable state. In simple terms, the photocurrent repetitive cycle includes four processes: rapid separation, slow decay, steady state, and rapid reorganization (Wang et al., 2014). To evaluate the PEC performance of the prepared material, the photocurrent responses of the (a) P5FIn, (b) P5FIn/Au, (c) erGO/P5FIn/Au are recorded in Fig. 2A. Photocurrent of the P5FIn/Au composites (curve b) is 3.5 times stronger than P5FIn (curve a). This might be ascribed to the broad light absorption range of Au, which improves the light utilization of nanocomposites. When erGO is introduced into this system, the photocurrent of the nanocomposites is 4.2 times higher than P5FIn (curve c). This can be attributed to the role of erGO with high conductivity, effectively hindering the recombination of photogenerated electron-hole pairs of nanocomposites.

Fig. 2B describes the electron transfer mechanism of erGO/P5FIn/Au photoelectrode. The energy level of erGO/P5FIn/Au nanocomposites is calculated by UV-visible spectral data (Wang et al., 2018; Jian et al., 2018). Under light irradiation, photogenerated electrons of P5FIn are transferred to the LUMO level while the photogenerated holes are moved to HOMO level. Then the erGO can accelerate photogenerated electrons transfer from P5FIn to the electron acceptor (O_2), improving the separation of electron-hole pairs. At the same time, the electrons from the ITO electrode are rapidly replenished into the photogenerated holes of P5FIn through Au. In this process, the nanocomposites generate strong photocurrent response as a result of the high conductivity of erGO and Au.

Electrochemical impedance spectroscopy (EIS) is an effective tool to characterize the interface properties of electrode (An et al., 2010), especially for the step-by-step construction process of photoelectrochemical sensors. 5.0 mM $[Fe(CN)_6]^{3/4+}$ solution is used for the test, with frequencies ranging from 0.1 Hz to 10000 Hz. The semicircle diameter of the EIS diagram represents the electron transfer resistance (R_{et}) value. As shown in Fig. 2C, the blank ITO electrode has a small semicircle diameter (curve a). The P5FIn/Au nanocomposites shows a larger semicircle diameter (curve b) compared with the blank ITO electrode because P5FIn/Au nanocomposites can inhibit the electron transfer at the interface. After erGO is introduced into the P5FIn/Au nanocomposites, there is a decrease in the diameter of the semicircle (curve c) compared with the curve b. This can be attributed to the high electron transfer ability of erGO. Therefore, it can be concluded that erGO/P5FIn/Au/ITO electrode is successfully prepared. The semicircle diameter of the EIS diagrams increases rapidly (curve d) after the aptamer is added onto the electrode. Due to the π-conjugated structure of erGO, the aptamer can be facilely immobilized on the surface of erGO through π-π stacking interaction between the nucleobases of DNA and erGO (Li et al., 2014a,b). When the modified electrode is incubated with AFB1 (50 ng mL^{-1}), the semicircle diameter of the EIS spectrum is decreased (curve e). This can be attributed to the AFB1 aptamer chain detached from the electrode surface. These results confirm that the aptamer chain is successfully combined with this nanocomposite.

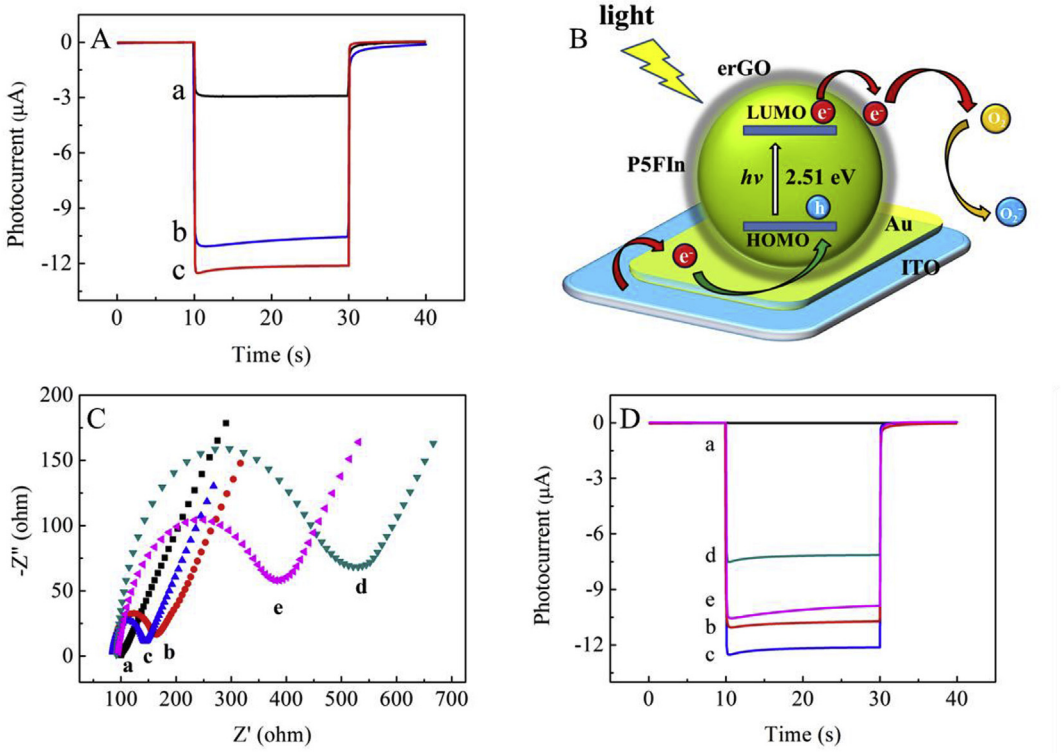

Fig. 2. (A) PEC responses of (a) P5FIn/ITO, (b) P5FIn/Au/ITO, and (c) erGO/P5FIn/Au/ITO in 0.1 M PBS (pH 7.4). (B) The photocurrent generation mechanism of erGO/P5FIn/Au modified electrode. (C) EIS and (D) time-based photocurrent response curves of the modified ITO electrodes (a) bare ITO, (b) P5FIn/Au/ITO, (c) erGO/P5FIn/Au/ITO, (d) aptamer/erGO/P5FIn/Au/ITO, (e) AFB1/aptamer/erGO/P5FIn/Au/ITO.

The PEC aptasensor construction process is also characterized by photocurrent response. As shown in Fig. 2D, there is a tiny photocurrent signal of blank ITO electrode (curve a). When P5FIn/Au is modified on the surface, a strong photocurrent signal (curve b) is occurred due to the good photoactivity of the nanocomposites. Subsequently, after erGO is modified to the surface of the electrode, the photocurrent signal is further enhanced (curve c) due to the high electron transfer capability of erGO. When the aptamer chain ssDNA is modified to the electrode surface, the photocurrent signal is reduced (curve d). ssDNA stand can hinder the electron transfer which results in a reduced separation rate of photogenerated hole-electron pairs. This result further prove that the aptamer chain is successfully immobilized on erGO surface by π-π stacking interaction between the carbon six-membered ring in graphene and the C-N heterocyclic ring in nucleobases of ssDNA (Antony and Grimme, 2008). When the modified electrode is incubated with AFB1 (50 ng mL^{-1}), the aptamer chain is detached from the surface of erGO and bound specifically to AFB1. This results in the increase of photocurrent. During this process, the sensor signal changes from "OFF" to "ON" (curve e). The data of EIS and photocurrent response indicate that the aptasensor is successfully constructed.

3.3. Optimization of experimental conditions

During the construction of PEC aptasensor, it is necessary to optimize their construction parameters. The details of experimental optimization are described in the Supporting Information. As shown in Fig. S1, the best experimental conditions are as follows: (A) 5 μM of aptamer chain concentration is used as the optimal concentration, (B) the incubation time of 70 min is chosen as the optimal time, (C) the optimal pH value of PBS is chosen as 7.4.

3.4. PEC detection for AFB1

The PEC aptasensor is used to detect AFB1 under optimal conditions. When the target analyte is absent, the aptasensor signal is "OFF" because of the hindering effect of ssDNA on electron transport. When the target analyte is present, the aptamer chain will be bound with the target analyte and automatically detach from the modified electrode surface. Thus, the aptasensor signal is "ON" now. As shown in Fig. 3A, the photocurrent intensity gradually increases with the increased concentration of AFB1. In addition, the photocurrent variation ($\Delta I = |I_{off} - I_{on}|$) shows a good linear relationship with the logarithm of the AFB1 concentration. As shown in Fig. 3B, the linear detection range (LDR) is 0.01 ng mL^{-1} to 100 ng mL^{-1}. The linear correlation equation is $y = 9.3737 + 0.7319\times$. The linear correlation coefficient $R^2 = 0.9912$. The limit of detection (LOD) of this aptasensor is 0.002 ng mL^{-1}, which is obtained from the 3σ calculation method (Armbruster and Pry, 2008).

Table 1
Comparisons with other reported methods for AFB1 detection.

Analytical methods	LDR (ng mL^{-1})	LOD (ng mL^{-1})	Reference
ECL	0.01–100	0.0039	Wang et al. (2018)
PEC	0.01–20	0.0021	Lin et al. (2017)
EIS	0.02–50	0.015	Wang et al. (2018)
CL	0.1–10	0.11	Shim et al. (2014)
DPV	0.05–6	0.05	Goud et al. (2017)
FRET	0.06–5	0.04	Xu et al. (2014)
Fluorescence	5–100	1.6	Chen et al. (2017)
Immunosensor	0.1–30	0.06	Ma et al. (2016)
Electrochemical	0.125–0.16	0.25	Goud et al. (2016)
PEC	0.01–100	0.002	this work

Table 1 summarizes the different analytical methods for AFB1 detection. For example, Wang et al. reports an ECL immunosensor for AFB1 detection with LDR from 0.01 ng mL^{-1} to 100 ng mL^{-1} and a LOD of 0.0039 ng mL^{-1} (Wang et al., 2018). Ma et al. develops an electrochemical (EC) immunosensor for AFB1 detection with a LDR from 0.1 ng mL^{-1} to 30 ng mL^{-1} and a LOD of 0.06 ng mL^{-1} (Ma et al., 2016). Compared with other works, this PEC aptasensor exhibits a wide linear range and a low limit detection. There are several reasons can account for this phenomenon. Firstly, under visible light irradiation a large amount of photogenerated electrons of the nanocomposites can be easily generated because of the narrow optical band gap of erGO/P5FIn/Au nanocomposites. Secondly, Au and erGO efficiently accelerate the transition of electrons, thus improving the photogenerated electronics separation rate of nanocomposites. Thirdly, this PEC "signal-on" type aptasensor has low background signal. Thus, this prepared PEC aptasensor shows a satisfied performance for AFB1 detection.

3.5. Stability, reproducibility and specificity studies

The stability of the constructed aptasensor is assessed by measuring 10 ng mL^{-1} AFB1. The photocurrent response of the aptasensor is recorded in Fig. 4A. It can be seen that after 19 times ON/OFF cycles, there is no obvious change of photoelectric response value of the aptasensor. In addition, after the aptasensor is placed at 4 °C for 15 days, the photocurrent response value remains 93% of the initial value (Fig. 4B). This proves that the aptasensor has good cyclic stability and storage stability.

Selectivity is another important parameter for evaluating sensor performance. The aptasensor is further investigated by incubating with different interfering substances. As shown in Fig. 4C, the aptasensors are tested under the conditions of (a) blank, (b) ochratoxin A (OTA), (c)

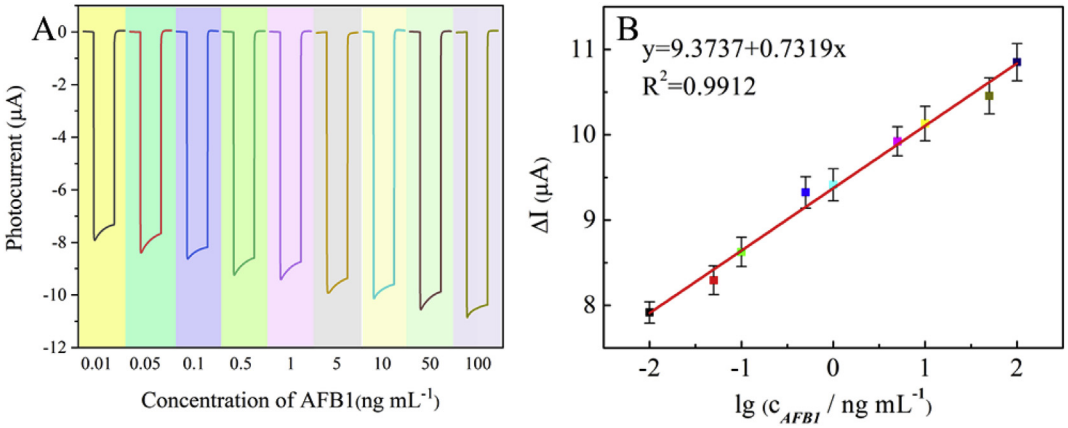

Fig. 3. (A) Photocurrent response and (B) calibration curve of the aptasensor to different concentrations of AFB1 (from 0.01 to 100 ng mL^{-1}). The error bars show the standard deviation of five parallel measurements.

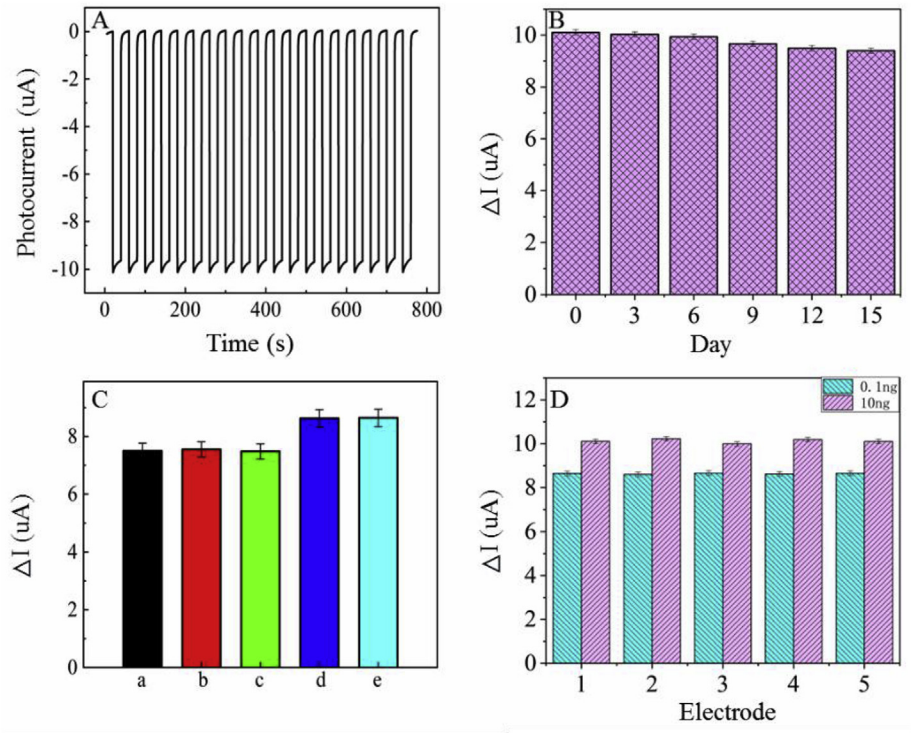

Fig. 4. (A) Photocurrent responses of the aptasensor for AFB1 (10 ng mL^{-1}). (B) The storage stability in the presence of AFB1 (10 ng mL^{-1}) evaluated every 3 days. (C) Selective testing of the aptasensor toward AFB1 detection in the (a) blank solution, (b) OTA, (c) FB1, (d) AFB1 (0.1 ng mL^{-1}), (e) their mixture (interferon concentration 10 ng mL^{-1}). (D) Repeatability of five electrodes to test the different concentrations of AFB1 (0.1 ng mL^{-1}, 10 ng mL^{-1}).

fumonisin B1 (FB1), (d) AFB1 (0.1 ng mL^{-1}), and (e) total mixing (interference concentration of 10 ng mL^{-1}), respectively. In the presence of sole interfering substances, the signal of the aptasensor is very close to the blank sample. When AFB1 is present, the aptasensor signal is significantly increased. Moreover, the photocurrent response of the mixed sample has no evident difference with the presence of AFB1 only. The experimental results show that the aptasensor has satisfactory selectivity for AFB1.

The repeatability of this aptasensor is also evaluated by the relative standard deviation (RSD). Two groups (5/group) of the same batch electrodes are used to detect different concentrations of AFB1 (0.1 ng mL^{-1}, 10 ng mL^{-1}), and the RSDs are calculated to be 2.3% and 3.6% (Fig. 4D). The RSDs of 3.2% and 3.8% are acquired when two groups (5/group) of different batches electrodes are used to detect the same sample under identical experimental conditions. The results indicate that the reproducibility and accuracy of PEC aptasensor are also satisfied.

3.6. Real samples analysis

The detection of actual samples is an important indicator for evaluating the practical application of the aptasensor. The aptasensor is used to analyze the as-prepared real samples. The performance of the aptasensor is evaluated by the recovery rate and relative standard deviation. As shown in Table S1, the concentration of AFB1 in the real peanuts and wheat samples are determined by using the PEC aptasensor. The recovery ranges from 98.3% to 106.7% in peanut and 97.2%–110.0% in wheat, and the RSDs ranges from 1.5% to 4.5% in peanut and 2.6%–5.0% in wheat. These results indicate that the aptasensor shows good accuracy in food samples analysis. Thus, the aptasensor may have potential application value in actual food detection.

4. Conclusions

In summary, a simple “signal-on” PEC aptasensor based on erGO/P5FIn/Au nanocomposites are developed for AFB1 detection. The introduction of Au nanoflower can further increase the separation of photogenerated electronics and improve the photocurrent signal. erGO can immobilize AFB1 aptamer chain by π-π stacking interaction. This PEC aptasensor shows a wide linear range and low detection limit for AFB1 due to good PEC performance of the nanocomposites and the “signal-on” design. The sensor also exhibits good stability, selectivity and rapid response. In addition, the PEC sensor has satisfactory detection results in the actual sample analysis. This work offers a new strategy for the PEC sensor construction based on CPs, and may provide potential applications for other food contamination detection.

Declaration of interests

The authors declare that they have no known competing financial interests or personal relationships that could have appeared to influence the work reported in this paper.

CRediT authorship contribution statement

Bin Zhang: Writing - original draft. **Yan Lu:** Formal analysis. **Chaonan Yang:** Investigation. **Qingfu Guo:** Methodology. **Guangming Nie:** Writing - review & editing, Conceptualization.

Acknowledgments

This work was financially supported by the National Natural Science Foundation of China (51373089), Natural Science Foundation of Shandong (ZR2011BM003) and Talent Fund of QUST (2018). The authors have declared that no conflict of interest exists.

Appendix A. Supplementary data

Supplementary data to this article can be found online at https://doi.org/10.1016/j.bios.2019.03.048.

References

An, Y., Tang, L., Jiang, X., Chen, H., Yang, M., Jin, L., Zhang, S., Wang, C., Zhang, W., 2010. Chem. Eur J. 16, 14439–14446.

Antony, J., Grimme, S., 2008. Phys. Chem. Chem. Phys. 10, 2722–2729.
Armbruster, D.A., Pry, T., 2008. Clin. Biochem. Rev. 29, S49–S52.
Chen, J., Zhao, G.C., 2017. Biosens. Bioelectron. 98, 155–160.
Chen, L., Wen, F., Li, M., Guo, X., Li, S., Zheng, N., Wang, J., 2017. Food Chem. 215, 377–382.
Fan, G.C., Han, L., Zhu, H., Zhang, J.R., Zhu, J.J., 2014. Anal. Chem. 86, 12398–12405.
Ge, L., Wang, P., Ge, S., Li, N., Yu, J., Yan, M., Huang, J., 2013. Anal. Chem. 85, 3961–3970.
Goud, K.Y., Catanante, G., Hayat, A., Satyanarayana, M., Gobi, K.V., Marty, J.L., 2016. Sens. Actuators B-Chem. 235, 466–473.
Goud, K.Y., Hayat, A., Catanante, G., Satyanarayana, M., Gobi, K.V., Marty, J.L., 2017. Electrochim. Acta 244, 96–103.
Groenendaal, L., Zotti, G., Aubert, P.H., Waybright, S.M., Reynolds, J.R., 2003. Adv. Mater. 15, 855–879.
Gu, B., Zhang, Q., 2018. Adv. Sci. 5 1700609.
Hao, N., Zhang, Y., Zhong, H., Zhou, Z., Hua, R., Qian, J., Liu, Q., Li, H., Wang, K., 2017. Anal. Chem. 89, 10133–10136.
Hou, Y., Qiu, M., Zhang, T., Ma, J., Liu, S., Zhuang, X., Yuan, C., Feng, X., 2017. Adv. Mater. 29 1604480.
Jian, N., Gu, H., Zhang, S., Liu, H., Qu, K., Chen, S., Liu, X., He, Y., Niu, G., Tai, S., Wang, J., Lu, B., Xu, J., Yu, Y., 2018. Electrochim. Acta 266, 263–275.
Kong, W., Wei, R., Logrieco, A.F., Wei, J., Wen, J., Xiao, X., Yang, M., 2014. Food Chem. 146, 320–326.
Li, R., Liu, Y., Li, X., Zhang, S., Wu, D., Zhang, Y., Wei, Q., Du, B., 2014a. Biosens. Bioelectron. 62, 315–319.
Li, R., Liu, Y., Cheng, L., Yang, C., Zhang, J., 2014b. Anal. Chem. 86, 9372–9375.
Li, L., Zhang, Y., Zhang, L., Ge, S., Liu, H., Ren, N., Yan, M., Yu, J., 2016. Anal. Chem. 88, 5369–5377.
Lin, Y., Zhou, Q., Tang, D., Niessner, R., Yang, H., Knopp, D., 2016. Anal. Chem. 88, 7858–7866.
Lin, Y., Zhou, Q., Tang, D., Niessner, R., Knopp, D., 2017. Anal. Chem. 89, 5637–5645.
Liu, B.H., Hsu, Y.T., Lu, C.C., Yu, F.Y., 2013. Food Control 30, 184–189.
Liu, Y., Ma, H., Zhang, Y., Pang, X., Fan, D., Wu, D., Wei, Q., 2016. Biosens. Bioelectron. 86, 439–445.
Liu, S., He, P., Hussain, S., Lu, H., Zhou, X., Lv, F., Liu, L., Dai, Z., Wang, S., 2018. ACS Appl. Mater. Interfaces 10, 6618–6623.
Lu, Z., Chen, X., Wang, Y., Zheng, X., Li, C.M., 2015. Microchim. Acta 182, 571–578.
Luo, X., Weaver, C.L., Tan, S., Cui, X.T., 2013. J. Mater. Chem. B 1, 1340–1348.
Ma, W., Han, D., Gan, S., Zhang, N., Liu, S., Wu, T., Zhang, Q., Dong, X., Niu, L., 2013. Chem. Commun. 49, 7842–7844.
Ma, H., Sun, J., Zhang, Y., Bian, C., Xia, S., Zhen, T., 2016a. Biosens. Bioelectron. 80, 222–229.
Ma, H., Sun, J., Zhang, Y., Bian, C., Xia, S., Zhen, T., 2016b. Biosens. Bioelectron. 80, 222–229.
Nie, G., Cai, T., Zhang, S., Bao, Q., Xu, J., 2007. Electrochim. Acta 52, 7097–7106.
Nie, G., Yang, H., Wang, S., Li, X., 2011. Crit. Rev. Solid State Mater. Sci. 36, 209–228.
Nie, G., Tang, Y., Zhang, B., Wang, Y., Guo, Q., 2018. Biosens. Bioelectron. 116, 60–66.
Pardo-Yissar, V., Katz, E., Wasserman, J., Willner, I., 2003. J. Am. Chem. Soc. 125, 622–623.
Shim, W.B., Mun, H., Joung, H.A., Ofori, J.A., Chung, D.H., Kim, M.G., 2014. Food Control 36, 30–35.
Spain, E., Keyes, T.E., Forster, R.J., 2013. Electrochim. Acta 109, 102–109.
Tang, D., Lin, Y., Zhou, Q., Lin, Y., Li, P., Niessner, R., Knopp, D., 2014. Anal. Chem. 86, 11451–11458.
Vasilescu, A., Marty, J.L., 2016. Trends Anal. Chem. 79, 60–70.
Wang, W.L., Xu, H., Chen, H.Z., Zheng, R.S., Tan, J., Zhan, R.T., Chen, W.W., 2013. China J. Chin. Mater. Med. 38, 1910–1914.
Wang, Y., Chu, W., Wang, S., Li, Z., Zeng, Y., Yan, S., Sun, Y., 2014. ACS Appl. Mater. Interfaces 6, 20197–20204.
Wang, Y., Zhao, G., Li, X., Liu, L., Cao, W., Wei, Q., 2018a. Biosens. Bioelectron. 101, 290–296.
Wang, Q., Ruan, Y.F., Zhao, W.W., Lin, P., Xu, J.J., Chen, H.Y., 2018b. Anal. Chem. 90, 3759–3765.
Wang, C., Qian, J., An, K., Ren, C., Lu, X., Hao, N., Liu, Q., Li, H., Huang, X., Wang, K., 2018c. Biosens. Bioelectron. 108, 69–75.
Xu, W., Xiong, Y., Lai, W., Yang, X., Li, C., Xie, M., 2014. Biosens. Bioelectron. 56, 144–150.
Zang, Y., Lei, J., Ju, H., 2017. Biosens. Bioelectron. 96, 8–16.
Zhang, D., Li, P., Yang, Y., Zhang, Q., Zhang, W., Xiao, Z., Ding, X., 2011. Talanta 85, 736–742.
Zhu, J., Huo, X., Liu, X., Ju, H., 2015. ACS Appl. Mater. Interfaces 8, 341–349.
Zhuang, J., Lai, W., Xu, M., Zhou, Q., Tang, D., 2015a. ACS Appl. Mater. Interfaces 7, 8330–8338.
Zhuang, J., Tang, D., Lai, W., Xu, M., Tang, D., 2015b. Anal. Chem. 87, 9473–9480.